Chapter 5

Planar Antennas with Enhanced Bandwidth and Radiation Characteristics

Mohammad Alibakhshikenari,
Mohammad Naser-Moghadasi,
Ramazan Ali Sadeghzadeh, Bal Singh Virdee and
Ernesto Limiti

Additional information is available at the end of the chapter

http://dx.doi.org/10.5772/66381

Abstract

Wireless companies want next-generation gadgets to download at rates of gigabits per second. This is because there is an exponential growth in mobile traffic, however, existing digital networks and devices will not be efficient enough to handle this much growth. In order to realize this requirement, the next generation of wireless communication devices will need to operate over a much larger frequency bandwidth. In this chapter, novel wideband and ultra-wideband (UWB) antennas that are based on loading the back-ground plane of a monopole radiator with concentric split-ring resonators are presented. It is shown that this modification improves the fractional bandwidth of the antenna from 41 to 87%; in particular, the operational bandwidth of the proposed antennas is double that of a conventional monopole antenna of the same size.

Keywords: split-ring resonator, ultra-wideband antenna, composite right/left-handed metamaterial, miniaturized antennas

1. Introduction

Multiband antennas for the personal wireless communications that facilitate various global communication standards and services have become imperative [1, 2]. The antennas for modern communication devices should be capable of operating at maximum possible frequency bands to serve multiple cellular and noncellular communication applications. Moreover, the antennas for portable handheld wireless communication terminals should have compact, low profile, robust, light weight, easy to manufacture, and flexible [3, 4].

The introduction of metamaterials (MTM) has provided unique and naturally nonexistent properties that have enabled the design of antennas with sizes much smaller than their conventional counterparts [5, 6]. Metamaterial structures can be realized using the resonant and nonresonant approaches [7, 8]. In particular, metamaterial structures can be implemented using the split-ring resonators (SRRs), complementary SRR (CSRRs), transmission-line-based structures, electric-field coupled-LC (ELC), etc. [9]. The properties of metamaterials are widely exploited to realize compact antennas with improved performance [10, 11]. Although resonant structures are inherently narrow band, a number of studies have been conducted to improve the bandwidth of metamaterial antennas [12, 13].

This chapter presents a number of antennas implemented with asymmetrical SRR loading and without SRR loading. The first version of antenna consists of a standard monopole radiator without SRR loading, and the second version comprises two monopoles with SRR loading. In effect, with the SRR loading, the bandwidth of the F-shaped and T-shaped antennas improves considerably. The F-shaped antenna's bandwidth improves from 31.5 to 75.4%, and in the case of the T-shaped antenna, the improvement is from 41.16 to 86.9% for VSWR ≤2. The SRR loading pulls down the resonant frequency so that both antennas cover the required frequency range related to worldwide interoperability for microwave access (WiMAX 3.5/5.5 GHz) and wireless local area network (WLAN 5.2/5.8 GHz) bands.

2. Antenna configurations

Two antennas with differing configurations with and without asymmetrical split-ring loading on the ground plane are shown in **Figures 1** and **2**, respectively. The F-shaped and T-shaped antenna structures are essentially monopole radiators. The second versions of the antennas were loaded with asymmetrical SRR on the ground plane to enhance their radiation characteristics. The ground planes of the antennas are truncated into L-shape with a notch.

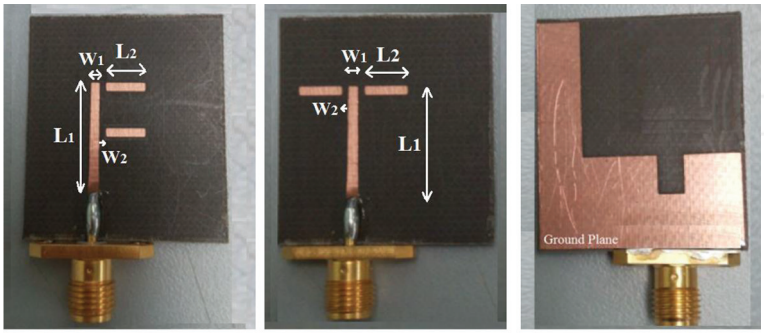

Figure 1. Fabricated prototypes of the monopole antennas, (a) top view of F-shaped antenna, (b) top view of T-shaped antenna, and (c) back view of both antennas without SRR loading. The antennas are in the *xy* plane.

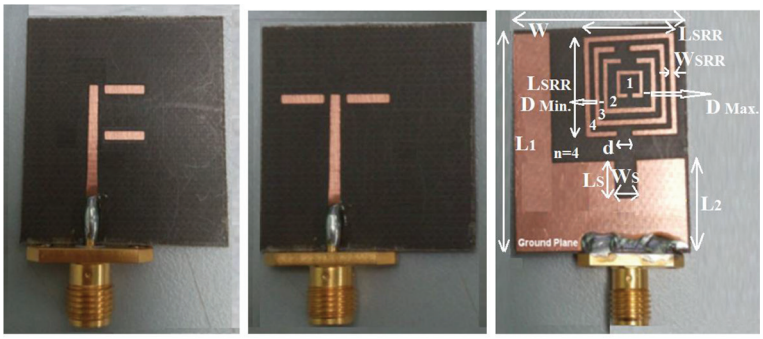

Figure 2. Fabricated prototypes of the antennas with asymmetrical SRR loading, (a) top view of F-shaped antenna, (b) top view of T-shaped antenna, and (c) back view of both antennas with SRR loading.

This configuration improved the antennas impedance matching. To validate the designs, the antenna structures were modeled and analyzed by Ansys 3D full-wave electromagnetic field simulator called high-frequency structure simulator (HFSS™) [14]. The antennas were optimized and fabricated on RT/duroid® 5880 substrate permittivity (ε_r) of 2.2, loss tangent (tanδ) of 0.002, and thickness (h) of 0.8 mm.

The dimensions of the parameters in **Figure 1** are as follows: L_1 = 19 mm, L_2 = 7 mm, W_1 = 1.4 mm, and W_2 = 0.4 mm. Dimensions in **Figure 2c** are as follows: L_{SRR} = 12 mm, W_{SRR} = 0.4 mm, D_{Min} = 0.4 mm, D_{Max} = 0.8 mm, d = 1.5 mm, L_1 = 30 mm, L_2 = 11 mm, W = 22 mm, L_S = 3.5 mm, and W_S = 2.2 mm. Overall size of the antennas are $25 \times 10^{-2}\lambda_o \times 11 \times 10^{-2}\lambda_o \times 2 \times 10^{-2}\lambda_o$ for F-shaped antenna and $25 \times 10^{-2}\lambda_o \times 21 \times 10^{-2}\lambda_o \times 2 \times 10^{-2}\lambda_o$ for T-shaped antenna, where the free space wavelength (λ_o) is 4 GHz. The performance of the antennas was verified using a network analyzer.

Asymmetrical split-ring resonator loading on the F-shaped and T-shaped antennas, shown in **Figure 2**, excites a lower resonance frequency mode that matches with the resonance frequency of monopole antennas, thus increasing the bandwidth of the antennas. As a result, the operational bandwidth of the antennas is extended to cover WiMAX (3.5–5.5 GHz) and WLAN (5.2–5.8 GHz) bands.

2.1. Results and discussion

The performance of the F-shaped and T-shaped antennas is compared with and without asymmetrical SRR loading. The simulated and measured reflection coefficient of the two antennas with and without SRR loading is shown in **Figure 3**. The simulated and measured impedance bandwidth of the F-shaped antenna without SRR loading is 1.62 GHz (3.95–5.57 GHz) and 1.5 GHz (4.0–5.50 GHz), respectively, which corresponds to a fractional bandwidth of 34.0 and 31.5%, respectively. The simulated and measured impedance bandwidth of the T-shaped antenna without SRR loading is 2.08 GHz (3.77–5.85 GHz) and 1.98 GHz (3.82–5.80 GHz), respectively, which corresponds to a fractional bandwidth of 43.24 and 41.16%, respectively. These results also show that there is excellent agreement in the simulated and measured results.

Results in **Figure 3** show that by loading the ground plane with SRR, a lower resonant frequency mode is excited in both antennas that match with the resonance frequency of monopole antennas. This has a consequence of increasing the bandwidth of the antennas. Simulation results using HFSS™ show that with SRR loading, the F-shaped and T-shaped antennas resonate at 3.65, 5.8 and 4.1, 5.9 GHz, respectively, and the measured resonant modes for the F-shaped and T-shaped antennas occur at 3.75, 5.9 GHz and 4, 6 GHz, respectively.

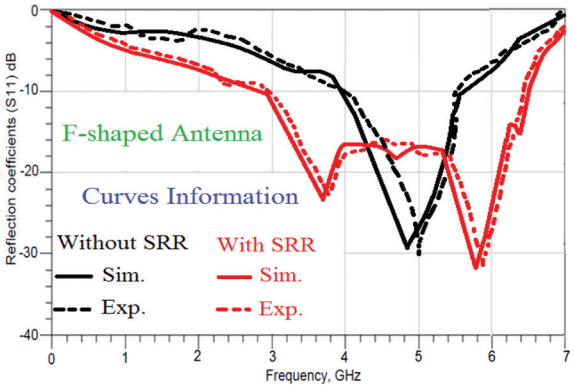

(a)

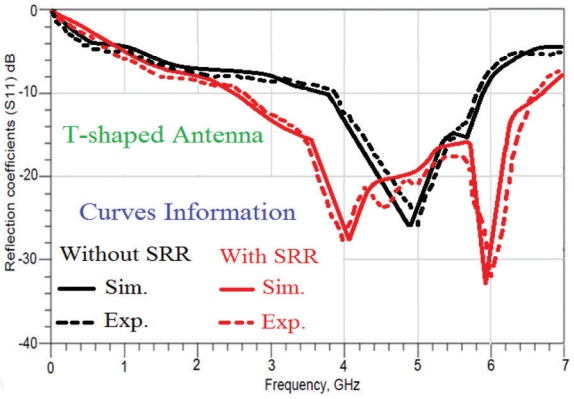

(b)

Figure 3. Simulated and measured reflection coefficient of (a) F-shaped and (b) T-shaped antennas with and without SRR loading.

It is evident from **Figure 3a** that the F-shaped antenna loaded with SRR has an impedance bandwidth of 78.27% (2.83–6.47 GHz) using HFSS™. The actual impedance bandwidth measured is 75.40% (2.9–6.41 GHz). Similar performance is obtained with the T-shaped antenna when loaded with SRR, as shown in **Figure 3b**. The simulated and measured impedance bandwidth of the SRR-loaded T-shaped antenna is 4.11 GHz (2.57–6.68 GHz) and 4 GHz (2.6–6.6 GHz), respectively, which corresponds to a fractional bandwidth of 88 and 87%, respectively. The operating frequency range of F-shaped and T-shaped antennas without

http://dx.doi.org/10.5772/66381

SRR using HFSS™ is centered at f_r = 4.80 and 4.85 GHz, respectively; however, the measured operating frequency range is centered at 5 GHz in both cases. The results show that with SRR loading on the ground plane of the antennas can considerably improve the bandwidth of both F-shaped and T-shaped antennas. Consequently, it is found that the SRR loading extends the impedance bandwidth of the monopole antennas enabling coverage across the WiMAX (3.5–5.5 GHz) and WLAN (5.2–5.8 GHz) bands.

For the unloaded antennas, the measured fractional bandwidth is 31.5% for the F-shaped antenna and 41.16% for the T-shaped antenna. With SRR loading, the fractional bandwidth improvement is 75.4% for the F-shaped antenna and 86.9% for the T-shaped antenna. There is clearly an improvement by a factor of 2.39 (F-shaped antenna) and 2.11 (T-shaped antenna).

The measured gain and radiation efficiency of the F-shaped and T-shaped antennas with and without the SRR loading is shown in **Figure 4a** and **b**, respectively, and salient features are given in **Table 1**.

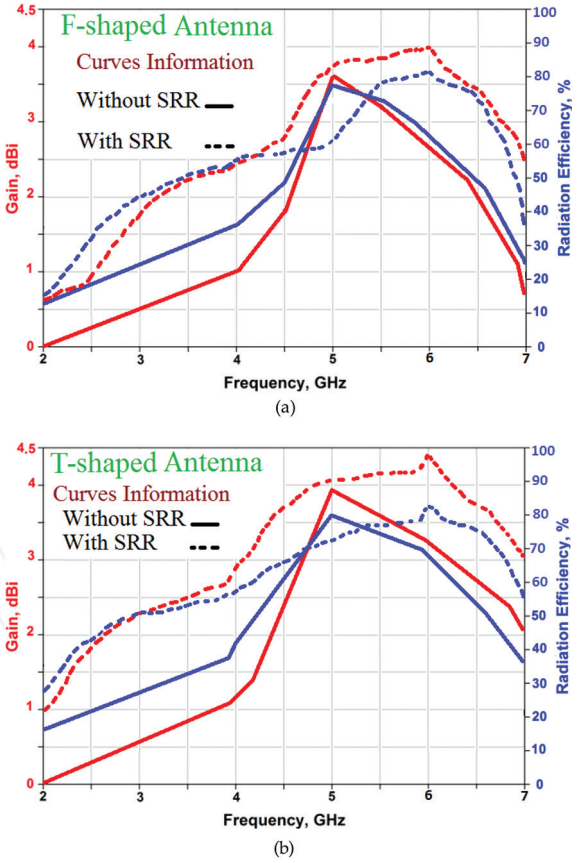

Figure 4. Measured gain and efficiency response of the two antennas with and without SRR loading. (a) F-shaped antenna and (b) T-shaped antenna.

		Without asymmetrical SRR loading	With asymmetrical SRR loading
F-shaped antenna	Gain (dBi)	@ 4, 4.5, **5**, 5.5 GHz: 1, 1.8, **3.6**, and 3.2	@ 2.9, 3.8, 5, **6**, 6.41 GHz: 1.7, 2.4, 3.7, **4**, 3.45
	Efficiency (%)	@ Same Freq.: 36.3, 48.1, **78.5**, 73.8	@ Same Freq.: 43.6, 51.7, 60.9, **81.2**, 76.5
T-shaped antenna	Gain (dBi)	@ 3.82, 4, **5**, 5.8 GHz: 1.15, 1.3, **3.9**, 3.3	@ 2.6, 3.82, 4, 5.8, **6**, 6.6 GHz: 1.8, 2.75, 2.9, 4.25, **4.4**, 3.7
	Efficiency (%)	@ Same Freq.: 36.5, 42.1, **80.2**, 70.4	@ Same Freq.: 45.5, 56.5, 58.9, 79.3, **82.6**, 75.4

Table 1. Radiation characteristics of the two antennas (*maximum values have been set as bold fonts*).

Figure 5a shows the two antennas radiate omni directionally in the E-plane across the entire operating frequency range in both cases of with and without SRR loading. Cross polarization is at least 15 dB below the main radiation. Both antennas radiate bidirectionally in the H-plane across their operating frequency. In this case, the cross polarization is also at least 15 dB below the main radiation. Results show that the gain is much stronger for both antennas with SRR loading at 6 GHz, and at 5 GHz, the gain is more pronounced only for the T-shaped antenna loaded with SRR.

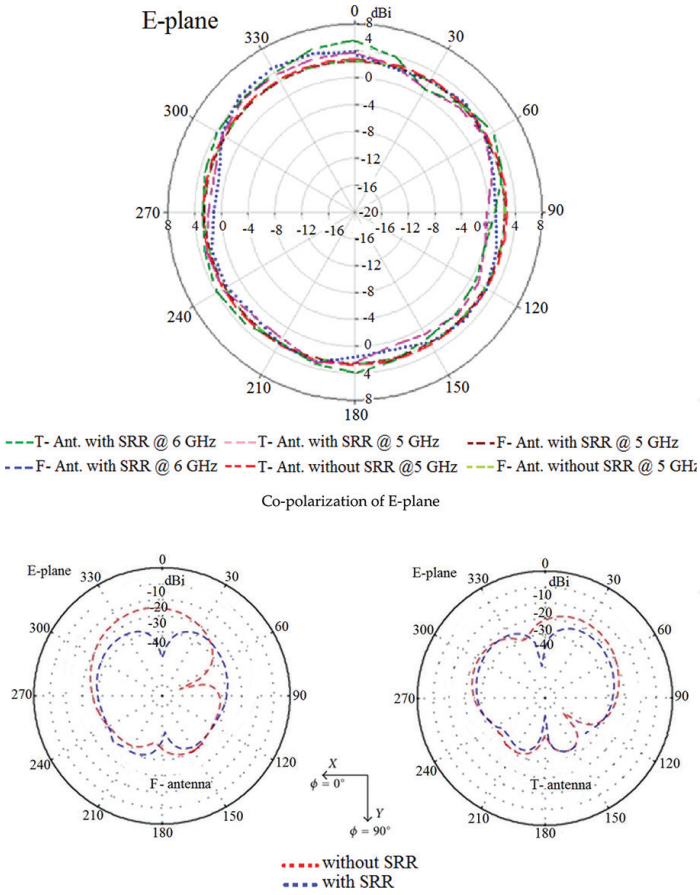

http://dx.doi.org/10.5772/66381

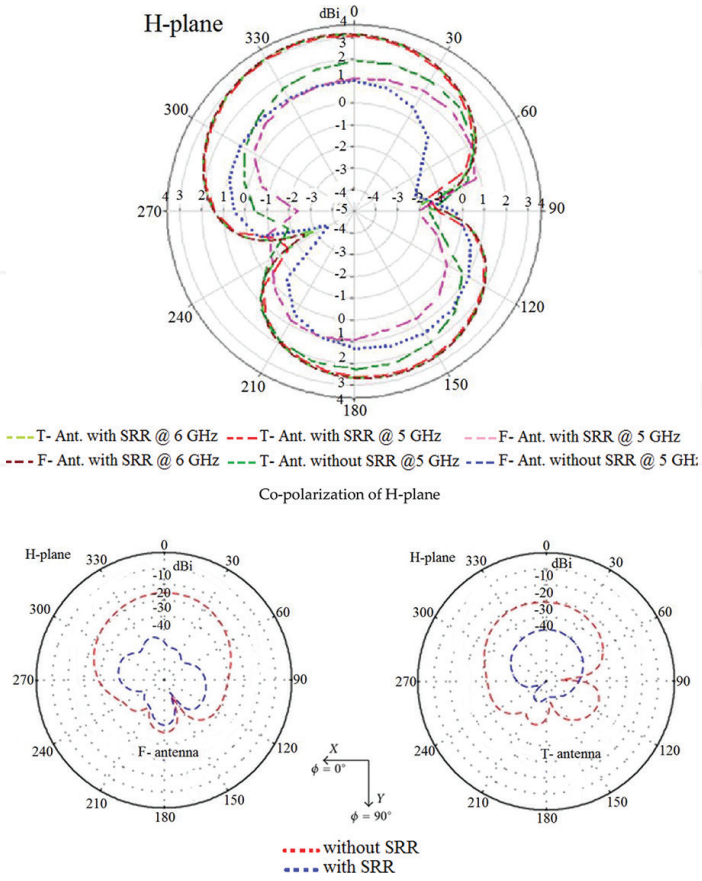

Figure 5. Measured E-plane and H-plane radiation patterns for F-shaped and T-shaped antennas with and without asymmetrical SRR loading at the operating frequencies. (a) Measured E-plane radiation patterns for F-shaped and T-shaped antennas. E-plane corresponds to Phi = 0°. (b) Measured H-plane radiation patterns for F-shaped and T-shaped antennas. H-plane corresponds to Theta = 90°. The slight shift in beam direction in H-plane is due to loading of SRR on the ground plane.

2.2. Effect of asymmetrical SRR loading

The propagation characteristics of the proposed structures are now considered by analyzing their dispersion properties. **Figure 6** shows the simplified discrete element equivalent circuit of the antenna structures. This electrical circuit is valid in the long-wavelength region (i.e., $\beta l \ll 1$). Note, β is the propagation constant for guided waves, and l is the length of the structure.

L (H/m) and C (F/m) represent the inductance and capacitance, respectively. These two reactance components define the inductance associated with the central conductor in the structures and the capacitive coupling between the structures and ground planes. SRR loading is modeled by a parallel resonant circuit constituted from inductance (L_S) and capacitance (C_S). The parallel resonant circuit is electromagnetically coupled to the structure through a mutual inductance (M). It can be shown that the dispersion relation is given by:

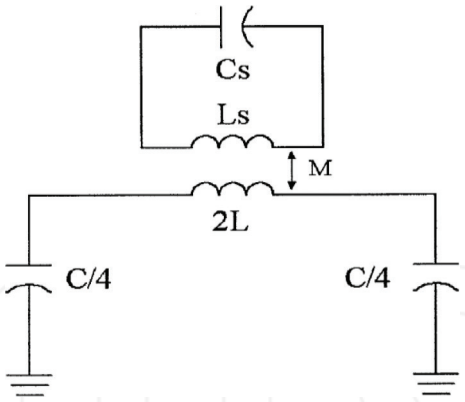

Figure 6. Lumped element equivalent circuit for the antenna structures.

$$\cos(\beta l) = 1 - \frac{LC\omega^2}{2} + \frac{C/C'_S}{4(1-\omega_0^2/\omega^2)} \tag{1}$$

$$C'_S = \frac{L_S}{M^2\omega_0^2} \tag{2}$$

$$L'_S = C_S M^2 \omega_0^2 \tag{3}$$

$$\omega_0^2 = \frac{1}{L_S C_S} = \frac{1}{L'_S C'_S} \tag{4}$$

M can be inferred from the fraction (A_f) of the slot area occupied by the rings according to:

$$M = 2L\,A_f \tag{5}$$

By obtaining the equivalent impedance of the series branch, the circuit can be simplified as shown in **Figure 7**. The dispersion relation for the circuit in **Figure 7** is given by [15]:

$$\cos(\beta l) = 1 - \left(\frac{L\omega - 1/C\omega}{4L/C}\right)\left(2L\omega - \frac{L'_S/C'_S}{L'_S\omega - 1/C'_S\omega}\right) \tag{6}$$

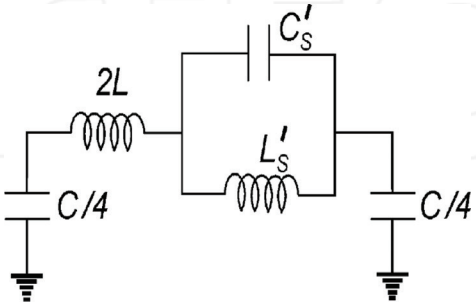

Figure 7. Simplified circuit with the series branch replaced by its equivalent impedance.

http://dx.doi.org/10.5772/66381

The dispersion diagram for the corresponding structures using HFSS™ and Eq. (6) is shown in an ω–β diagram in **Figure 8**. The circuit elements have been calculated for the antenna structures shown in **Figure 2**.

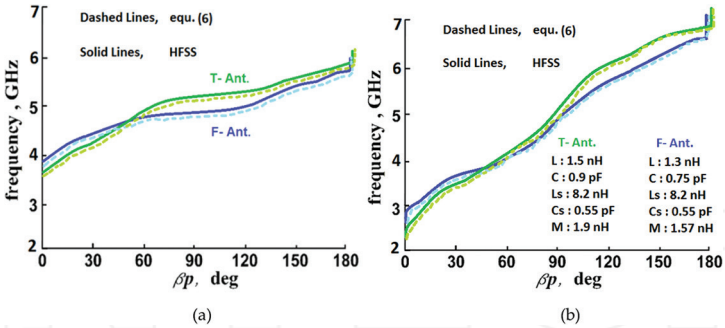

Figure 8. Dispersion diagram of the proposed F-shaped and T-shaped antennas. (Blue lines are for F-shaped antenna, and the green lines are for T-shaped antenna). (a) Without SRR loading and (b) loaded with SRR.

Nicolson-Ross-Weir method was used to obtain the permeability of the SRR [16]. Impedance and permeability response of F-shaped and T-shaped antennas loaded with SRR, shown in **Figure 9**, reveal that the impedance and permeability of the SRR in both antennas are positive and stable over the operating bands of antennas.

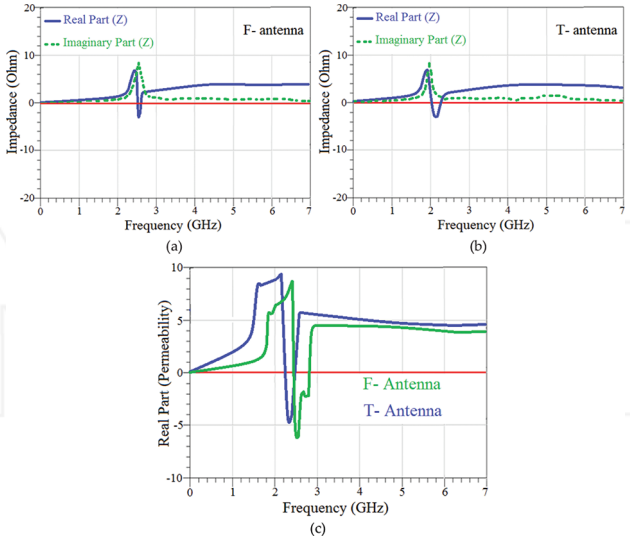

Figure 9. Impedance and permeability response for the two antennas loaded with SRR. (a) Impedance of the SRR for F-shaped antenna, (b) impedance of the SRR for T-shaped antenna and (c) permeability of the SRR for both antennas.

To achieve the desired performance from the antennas, it was necessary to optimize the dimensions of the asymmetrical SRR loading using Ansys HFSS™ EM Simulator. **Figures 10** and **11** show the effect of the SRR dimensions on the reflection coefficient response of the two antennas as a function of length (L_{SRR}), width (W_{SRR}), and gap between the SRR rings (D_{SRR}). Results show that when the length (L_{SRR}), width (W_{SRR}), and gap (D_{SRR}) of SRR loading are increased, the bandwidth of the antennas is marginally improved.

Effect on the antenna's gain and radiation efficiency as a function of the SRR dimensions is shown in **Figure 12**. These results clearly show the dimensions of the SRR greatly influences the antenna's the gain and efficiency properties over the entire operating frequency range of the antenna.

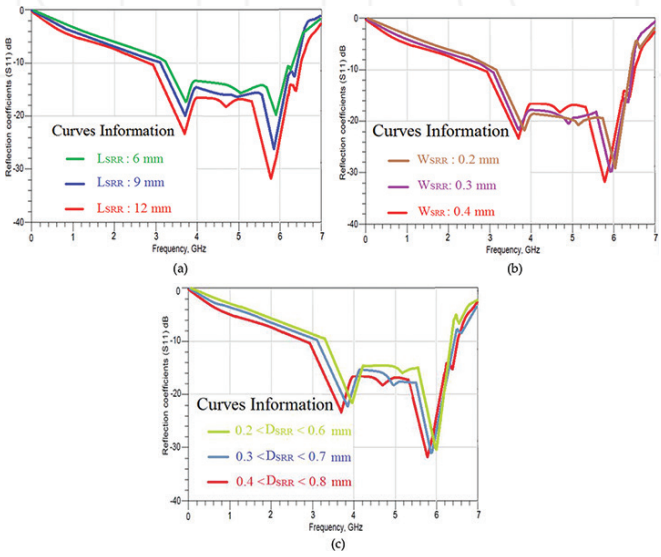

Figure 10. Parametric study on SRR dimensions for the F-shaped antenna. (a) Effect of SRR length (L_S) (all other parameters remain constant). (b) Effect of SRR width (W_S) (all other parameters remain constant). (c) Effect of gap between the rings of the SRR (D_{SRR}) (all other parameters remain constant).

3. Conclusion

To summarize, this chapter presented two monopole antenna configurations loaded with and without split-ring resonators (SRR). The results presented show that SRR loading improves the antenna's performance in terms of bandwidth and radiation characteristics compared to conventional unloaded monopole antennas. This is because SRR-loaded antennas excite a lower resonance frequency mode that matches with the resonance frequency of the monopoles, thereby extending the overall impedance bandwidths. The metamaterial antenna presented is implemented with CRLH-TL unit-cells comprising "LT-shaped" slots in a radiating patch with an inductive spiral ground through a via

http://dx.doi.org/10.5772/66381

hole. The SRR-loaded antennas operate over a frequency range that covers WiMAX (3.5/5.5 GHz) and WLAN (5.2/5.8 GHz) bands. The antennas are relatively small and have a size of 0.29 λ_o × 0.21 λ_o where λ_o is 2.9 GHz. The antenna has a maximum gain and radiation efficiency of 4.4 dBi and 82.6%, respectively, at 6 GHz. The metamaterial antenna covers a frequency bandwidth extending from 0.5 to 11.3 GHz for VSWR < 2 and has a size of 22.6 × 5.8 × 0.8 mm^3. It has a maximum gain and radiation efficiency of 6.5 dBi and 88%, respectively, at 8 GHz.

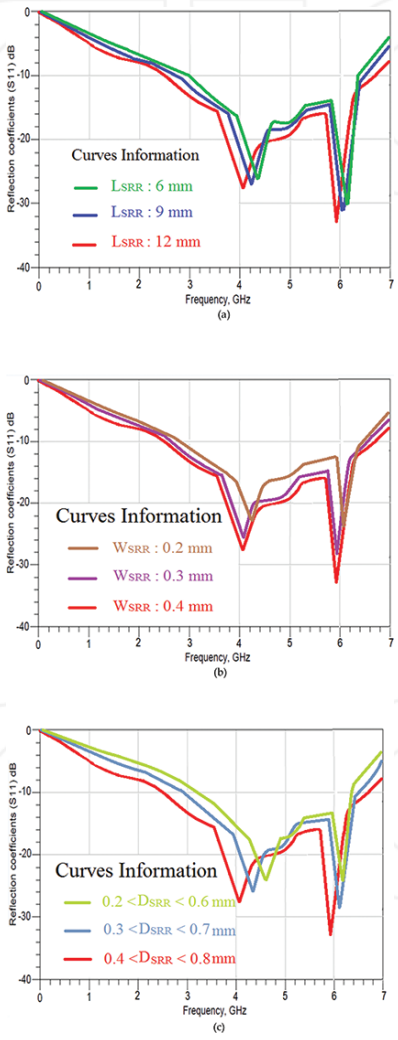

Figure 11. Parametric study on SRR dimensions for the T-shaped antenna. (a) Effect of SRR length (L_S) on the reflection coefficient response (all other parameters remain constant). (b) Effect of SRR width (W_S) on the reflection coefficient response (all other parameters remain constant). (c) Effect of varying the gap between the rings of the SRR (D_{SRR}) on reflection coefficient response (all other parameters remain constant). The number of SRR pairs used is four.

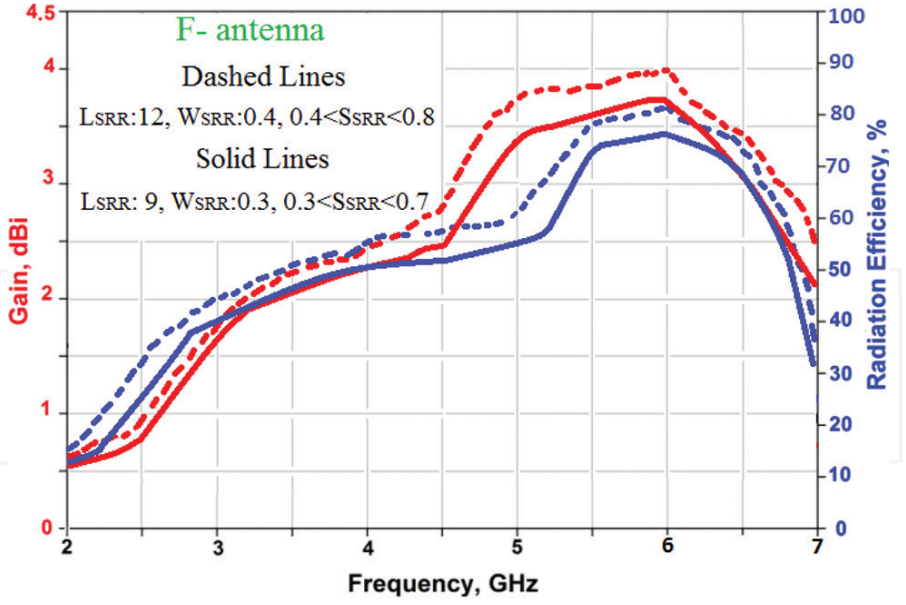

(a)

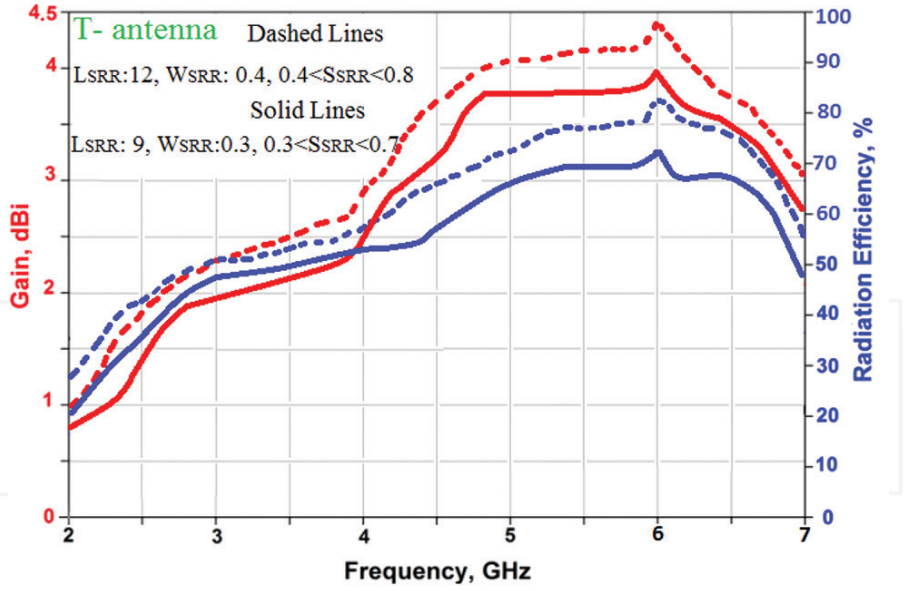

(b)

Figure 12. Effect on the radiation characteristics of the two antennas by the dimensions of SRR loading. (a) F-shaped antenna and (b) T-shaped antenna.

Acknowledgements

The Authors would like to give their special thanks to faculty of microelectronics for the financial support.

Author details

Mohammad Alibakhshikenari[1]*, Mohammad Naser-Moghadasi[2], Ramazan Ali Sadeghzadeh[3], Bal Singh Virdee[4] and Ernesto Limiti[1]

*Address all correspondence to: Alibakhshikenari@ing.uniroma2.it

1 Department of Electronic Engineering, University of Rome Tor Vergata, Rome, Italy

2 Faculty of Engineering, Science and Research Branch, Islamic Azad University, Tehran, Iran

3 Faculty of Electrical Engineering, K. N. Toosi University of Technology, Tehran, Iran

4 Center for Communications Technology, London Metropolitan University, London, UK

References

[1] Y. Jee, Y.M. Seo, "Triple-band CPW-fed compact monopole antennas for GSM/PCS/DCS/WCDMA applications," *Electron Lett*, 2009; 45(9): 446–448. doi:10.1049/el.2009.3383

[2] C.T. Lee, K.L. Wong, "Uniplanar printed coupled-fed PIFA with a band-notching slit for WLAN/WiMAX operation in the laptop computer," *IEEE Trans Ant Propag*, 2009; 57(4): 1252–1258. doi:10.1109/TAP.2009.2015843

[3] L. Jofre, B.A. Cetiner, F. De Flaviis, "Miniature multi-element antenna for wireless communications," *IEEE Trans Ant Propag*, 2002; 50(5): 658–669. doi:10.1109/TAP.2002.1011232

[4] M. Alibakhshi-Kenari, "Printed planar patch antennas based on metamaterial,"*Int J Electron Lett*, 2014; 37–42. doi:10.1080/21681724.2013.874042

[5] A. Lai, C. Caloz, T. Itoh, "Composite right/left-handed transmission line metamaterials", *IEEE Microw Mag*, 2004; 5(3): 34–50. doi:10.1109/MMW.2004.1337766

[6] C.J. Lee, K.M.K.H. Leong, T. Itoh, "Composite right/left-handed transmission line based compact resonant antennas for RF module integration," *IEEE Trans Ant Propag*, 2006; 54(8): 2283–2291. doi:10.1109/TAP.2006.879199

[7] Christophe Caloz, Tatsuo Itoh, "*Electromagnetic Metamaterials: Transmission Line Theory and Microwave Applications*", ISBN: 978-0-471-66985-2, 376 pages, December 2005, Wiley-IEEE Press.

[8] C. Caloz, T. Itoh, A. Rennings, "CRLH metamaterial leaky-wave and resonant antennas," *IEEE Ant Propag Mag*, 2008; 50(5): 25–39. doi:10.1109/MAP.2008.4674709

[9] A. Alu, F. Bilotti, N. Engheta, L. Vegni, "Sub-wavelength, compact, resonant patch antennas loaded with metamaterials," *IEEE Trans Ant Propag*, 2007; 55(1): 13–25. doi:10.1109/TAP.2006.888401

[10] C. Caloz, T. Itoh, "Novel microwave devices and structures based on the transmission line approach of meta-materials", *Microwave Symposium Digest, 2003 IEEE MTT-S International*, 8-13 June 2003, Pennsylvania Convention Center Philadelphia, Pennsylvania.

[11] M. Schussler, J. Freese, R. Jakoby, "Design of compact planar antennas using LH-transmission lines", Microwave Symposium Digest, 2004 IEEE MTT-S International, 6-11 June 2004.

[12] Mohammad Alibakhshikenari, Mohammad Naser-Moghadasi, R.A. Sadeghzadeh, Bal S. Virdee, Ernesto Limiti, "Traveling-wave antenna based on metamaterial transmission line structure for use in multiple wireless communication applications", AEU - International Journal of Electronics and Communications, Volume 70, Issue 12, December 2016, Pages 1645–1650.

[13] Mohammad Alibakhshikenari, Mohammad Naser-Moghadasi, R.A. Sadeghzadeh, Bal S. Virdee, Ernesto Limiti, "Miniature CRLH-based ultra wideband antenna with gain enhancement for wireless communication applications", ICT Express, Volume 2, Issue 2, June 2016, Pages 75–79.

[14] Ansoft HFSS, www.ansoft.com/products/hf/hfss.

[15] David M. Pozar, "Microwave Engineering, 4th Edition", December 2011, Wiley.

[16] R.W. Ziolkowski, "Design, fabrication, and testing of double negative metamaterials," *IEEE Trans Ant Propag*, 2003; 51: 1516–1529. doi:10.1109/TAP.2003.813622